Systems & Control Transactions

Research Article - Peer Reviewed Conference Proceeding
ESCAPE 35 - European Symposium on Computer Aided Process Engineering
Ghent, Belgium. 6-9 July 2025
Jan F.M. Van Impe, Grégoire Léonard, Satyajeet S. Bhonsale,
Monika E. Polańska, Filip Logist (Eds.)

PSE PRESS

Structural Optimization of Translucent Monolith Reactors through Multi-objective Bayesian Optimization

Onur C. Boy[a], Ulderico Di Caprio[a], Idelfonso B.R. Nogueira[b] and M. Enis Leblebici[a]*

[a] KU Leuven, Center for Industrial Process Technology, Diepenbeek, Belgium
[b] Norwegian University of Science and Technology (NTNU), Department of Chemical Engineering, Trondheim, Norway
* Corresponding Author: muminenis.leblebici@kuleuven.be

ABSTRACT

Photochemical monolith reactors offer advantages over microreactors by providing high mixing efficiency and surface area to volume ratio while being scalable. However, optimizing monolith design parameters like channel number, shape, and stacking is critical to maximizing light usage and reactor efficiency. This work proposes using Bayesian optimization and COMSOL Multiphysics simulations to automatically design translucent monoliths for photochemical reactions. The goal is to maximize both photochemical space-time yield and space-time yield. Ray tracing simulations were performed while evaluating five different channel geometries (circular, elliptical, triangular, square, and pentagonal) and optimizing parameters, including channel diameter, vertical stacking, shape rotation, and ellipse axis ratio. Results showed a clear trade-off between Space-Time Yield (STY) and Photochemical Space-Time Yield (PSTY), with optimized elliptical channels achieving up to 15.3% improvement in STY with minimal PSTY increase and 9.0% enhancement in PSTY with negligible STY decrease.

Keywords: Photochemistry, Photoreactors, Ray tracing, Bayesian Optimization, Monoliths

INTRODUCTION

Photochemical reactors harness light energy to drive chemical transformation under mild conditions with high energy efficiency [1]. Despite their numerous advantages, including enhanced selectivity and control, reduced organic solvent requirements, renewable energy utilization, and access to novel reaction pathways, industrial adoption remains limited due to several key challenges [2]. The primary obstacles include suboptimal apparent reaction rates, insufficient energy efficiency, and reactor design limitations that impede effective scale-up largely arising from limited light penetration into the reaction environment, leading to low light utilization [3]. While microreactors can partially address these limitations through high surface area-to-volume ratios and improved illumination uniformity [4], their restricted throughput capacity and spatial mismatch between the light source and the reactor channels present significant barriers to industrial implementation. Consequently, there is a pressing need for innovative reactor designs that can effectively balance photon distribution, mass transfer, and scalability considerations.

Monolith reactors offer a scalable approach combining microreactor advantages with industrial throughput. While microreactors excel in mass and photon transfer due to high surface area-to-volume ratios, their scalability limits industrial use. Translucent monolithic structures overcome these limitations, enabling efficient light penetration across reaction channels and achieving substantially higher energy efficiency than conventional designs [6]. However, optimal geometry and opacity are crucial to prevent non-uniform light distribution between surface and reaction regions.

Light scattering in photochemical reactors significantly influences reactor performance through complex light-matter interactions [7]. The geometry of reactor channels, particularly their diameter and spatial arrangement, plays a crucial role in determining photon distribution and utilization efficiency [8].

Ray-tracing simulations can accurately predict photon distribution patterns within a reactor volume. Several studies in the literature have employed ray tracing to optimize the geometrical configurations of photoreactor

systems. Singh et al. conducted a parametric study to optimize the geometry of a photocatalytic monolith reactor, focusing on the optimal aspect ratio of channels and the lamp-to-monolith distance, achieving a maximum photon efficiency of 50% [9]. Athanasiou et al. optimized a photocatalytic reactor design integrating membranes and optical fibers for water purification [10]. Their study identified an optimal intermediate channel thickness of 2 mm, enabling the treatment of 50 m^3/day of water with a pressure drop of 1.5 bar. In another study, Martín-Somer et al. investigated reflector geometries for a tubular UV reactor [11]. They demonstrated that parabolic reflectors achieved the highest optical efficiency (65.9%). Jacobs et al. developed translucent monoliths for the degradation of pharmaceutical micropollutants during wastewater treatment. Using COMSOL ray tracing, they optimized the design with 2 mm channel diameter, 2 mm spacing, and 3 vertically stacked rows of channels. The optimized reactor showed significantly improved energy efficiency compared to conventional internally illuminated monoliths [6].

Coupling ray tracing simulations with a gradient-free optimization algorithm, such as Bayesian optimization (BO), can enable the automated design of photochemical reactors. BO can systematically navigate multiple design variables simultaneously - including channel geometry, dimensions, and orientation - while minimizing the number of required simulations. This combined approach offers several advantages over classical optimization approaches where parameter sweep analysis is employed for addressing complex geometrical configurations. These advantages include a continuous design space, rapid identification of optimal design parameters, efficient exploration in high dimensional spaces, and a significant reduction in the experimental effort required for reactor design [12]. Moreover, the flexibility and extensibility of the coupled approach make the optimization process adaptable to various photocatalytic reactor design problems, allowing for the incorporation of additional physical models and design variables.

In this study, the multi-objective optimization of translucent monolithic structures is investigated using ray tracing simulation and Bayesian optimization to maximize the efficiency of the reactor previously studied by Jacobs et al. [6]. To the best of our knowledge, this is the first study to couple ray tracing simulations with Bayesian optimization. The objective function is linearized through space-time yield (STY) and photochemical space-time yield (PSTY) to balance reactor efficiency and energy efficiency, respectively. The effect of weights assigned to STY and PSTY on the optimal configuration is also examined through varying weights. Six channel geometries (circular, elliptic, triangular, square, and pentagonal) are examined along with channel rotation, number of vertically stacked rows, channel diameter, and aspect ratio.

METHODOLOGY

Ray Tracing Simulation

COMSOL Multiphysics 6.2 employs nonsequential ray tracing to model complex light-matter interactions in photochemical reactors. The algorithm solves coupled first-order ordinary differential equations for ray position (q) and wave vector (z) components:

$$\frac{dz}{dt} = -\frac{\partial w}{\partial q} \quad (1)$$

$$\frac{dq}{dt} = -\frac{\partial w}{\partial z} \quad (2)$$

The simulation begins by discretizing the geometry and establishing initial ray positions and directions. Primary rays are generated from a source, and when these rays encounter interfaces with different refractive indices, the algorithm computes new directions based on Snell's law and Fresnel's equations: Snell's law describes how light bends when passing between two mediums defined by n_1 and n_2, and the refractive indices of the two mediums, $\theta_1$and θ_2, the angles of incidence and refraction. Fresnel's equations quantify how much light is reflected and how much is transmitted (refracted) at an interface between two media defined by reflection and transmission coefficients.

Figure 1 shows the 2D geometry of a monolith design example used in this study, implemented in COMSOL, including elliptic channel geometries. The refractive index of the reaction medium is determined by the concentration of photocatalyst, which is 0.0125 mol TiO_2/m^3 Water. The wall condition at the outer border of the reactor is set to deactivate any rays that exit the reactor. Number of rays per release is set to 100, and rays are realesed with a canonical ray direction vector with a cone angle of π/6 from the boundary release as it is depicted in Figure 1. The total source power per unit thickness is 50 W/m. Lastly, a deposited ray power is located on channel surfaces to capture the amount of absorbed light by the reaction medium.

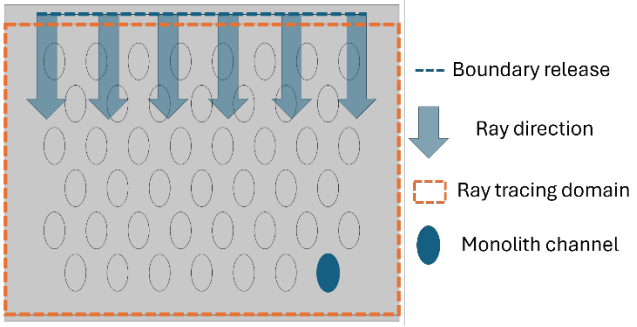

Figure 1. 2D geometry of the monolith reactor.

The maximum number of secondary rays was limited to 500,000 to prevent memory overflow. Optimal number

of mesh density is chosen to be the same with Jacobs et al. [6]. A lower limit threshold is also employed to discard secondary rays fall below a certain amount of energy. Table 1 shows the parameters set in the simulation:

Table 1: Parameters of ray tracing simulation employed in this work

Ray tracing parameters	Value
Mesh density	70 elements per mm^3
Number of primary rays	10,000
Limit for secondary rays	500,000
Refractive index of the 3D-printed material	1.5403
Refractive index of air	1
Refractive index of TiO_2-Water suspension	1.335
Wavelength of the Light	550 nm
Source power per unit thickness	50 W/m
Ray release cone angle	π /6

Theoretical Framework

The evaluation of different reactor designs requires a comprehensive thinking on both energy efficiency and reactor performance, as indicated by PSTY and STY, respectively. The energy of a single photon, E_{photon} [J], can be expressed as where v is the speed of light, h is Planck's constant, and λ is the wavelength of the absorbed light

$$E_{photon} = \frac{v \cdot h}{\lambda} \quad (3)$$

then, the total amount of absorbed photonic energy divided by the energy of a single photon gives the number of photons absorbed, ϑ, which can be expressed as:

$$\vartheta = \frac{P_{abs}}{E_{photon}} \quad (4)$$

where P_{abs} is the absorbed power by the reaction medium, which is obtained from simulation by integrating deposited power over channel surfaces. Further, dividing ϑ to Avogadro's number, N_A, gives the moles of absorbed photons in $mol \cdot s^{-1}$:

$$\vartheta = \frac{P_{abs} \cdot \lambda}{v \cdot h \cdot N_A} \quad (5)$$

STY is defined as the amount of treated wastewater per unit volume of the reactor. In this study, the quantum yield is assumed to be 2.35%, representing the fraction of absorbed photons that actively contribute to the photodegradation process. To calculate the actual rate of pollutant degradation, the quantum yield is multiplied by the number of absorbed photons (in $mol \cdot s^{-1}$). Once the pollutant degradation rate is obtained, the volume of treated water, expressed in m^3 $water.s^{-1}$, can be calculated by dividing the pollutant degradation rate by the pollutant concentration, $C_{pollutant}$ (in m^3 $water.s^{-1}$). The value of $C_{pollutant}$ is taken as 0.1 $mol.m^3$ $water^{-1}$. Then, STY (in m^3 water. m^3 $reactor^{-1}.s^{-1}$), is determined by normalizing this treated water volume by the reactor volume, $V_{reactor}$:

$$STY = \frac{\vartheta \cdot \Phi}{C_{pollutant} \cdot V_{reactor}} \quad (6)$$

Consequently, $PSTY$ is calculated by dividing STY to normalized lamp power, P_{norm} (W). $PSTY$ considers how much energy spent for a unit volume of reactor, and normalized lamp power is calculated by dividing lamp power, P_{lamp}, to the reactor volume, $V_{reactor}$. $1\ m^3$ of reactor is taken as reference volume:

$$P_{norm} = \frac{P_{lamp}}{V_{reactor}} \times 1\ m^3 \quad (7)$$

$$PSTY = \frac{STY}{P_{norm}} \quad (8)$$

STY and $PSTY$ provide a robust framework to evaluate reactor designs, enabling a balanced assessment of energy efficiency and performance for optimized photoreactor operation.

Bayesian Optimization

Bayesian optimization is an efficient method for finding the global optimum of black-box functions that are expensive to evaluate. It combines a probabilistic surrogate model that approximates the objective function and provides uncertainty estimates with an acquisition function that determines the most promising points to evaluate next. The surrogate model is updated as new observations are made, continuously improving its predictions of the underlying function. The algorithm works iteratively by initializing with a few random samples and then fitting the surrogate model to the observed data. At each iteration, it selects the next evaluation point by maximizing an acquisition function that balances exploration (sampling uncertain regions) and exploitation (sampling regions likely to have good values). The acquisition function is a mathematical function used in BO, and it assigns a value to each potential point, indicating how valuable it would be to evaluate that point next.

Expected Improvement (EI) was chosen to guide the optimization process for the remainder of the study due to its adaptive behavior between exploration and exploitation. The loss function is defined as a linear combination of the normalized STY (STY_{norm}) and normalized PSTY ($PSTY_{norm}$), as shown in Equation 9. For the normalization process, initial estimates of the minimum and maximum values are based on prior knowledge.

$$Loss = w_{STY} \times STY_{norm} + w_{PSTY} \times PSTY_{norm} \quad (9)$$

$$STY_{norm} = \frac{STY - STY_{min}}{STY_{max} - STY_{min}} \quad (10)$$

$$PSTY_{norm} = \frac{PSTY - PSTY_{min}}{PSTY_{max} - PSTY_{min}} \quad (11)$$

To determine an appropriate weight set (w_{STY}, w_{PSTY}) for the objective function, the optimization algorithm is executed for varying weight values. The assigned weights range from 0.1 to 0.9, discretized in increments of 0.1, resulting in 9 different weight sets. Each run is initialized with 25 random configurations and iterated for an additional 75 simulations.

Table 2: Variables defining the geometry in the ray tracing simulation.

Variable	Domain	Range
Characteristic diameter	Real	1-6.5
Aspect ratio	Real	0.25-1.75
Number of vertically stacked rows	Integer	1,2,3
Channel Shape	Categorical	Elliptic, circular, square, triangular, pentagonal, plus-signed
Rotation	Real	0-90 degree

Variable space is defined as shown in Table 2. Six channel geometries (i.e., circular, elliptic, triangular, square, and pentagonal) are examined along with channel rotation, number of vertically stacked cell rows, characteristic channel diameter, and aspect ratio of ellipses. The characteristic diameter is defined as the diameter for circles, the minor axis length for ellipses, the side length for triangles and squares, and the side length of the cross frame for plus-shaped channels. Analyzed channel shapes are depicted in Figure 2. Python library *scikit-optimize* is utilized for the optimization study. After the simulation is loaded onto a Python interface using MPh v1.2.4, the optimization study is initialized with 25 random points and run for an additional 75 iterations. During each iteration, a COMSOL ray tracing simulation is executed for a new geometrical configuration. The resulting absorbed power is retrieved from the simulation, and the surrogate model is updated before the next evaluation point.

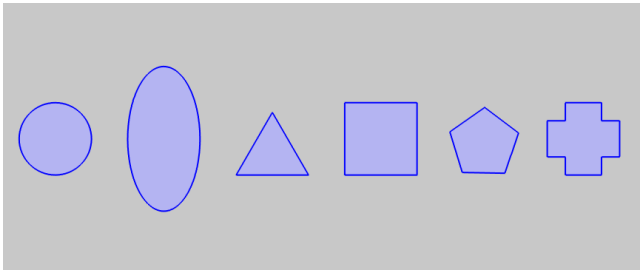

Figure 2. Candidate channel shapes

RESULTS AND DISCUSSION

The geometric configuration of each iteration is recorded, as each represents a valid reactor design. Figure 3 presents the best three solutions for each weight set, distinguished by unique color and marker combinations. As expected, when the weight of STY increases, the best solutions tend to cluster around the bottom-right corner of the figure, where STY is maximized. Conversely, assigning larger weights to PSTY causes the solutions to shift toward the upper-left corner of the figure, resulting in higher PSTY values and lower STY yields. This competing relationship between STY and PSTY is also evident in the figure. Consequently, more balanced solutions are obtained for weights w_{STY}=0.5 and w_{PSTY}=0.5. These weights are utilized for the remainder of the study. It should be noted that each run may yield different solutions due to the probabilistic nature of the optimization process. Nevertheless, the general trend is consistent across varying weights, and the selected weights are deemed reliable.

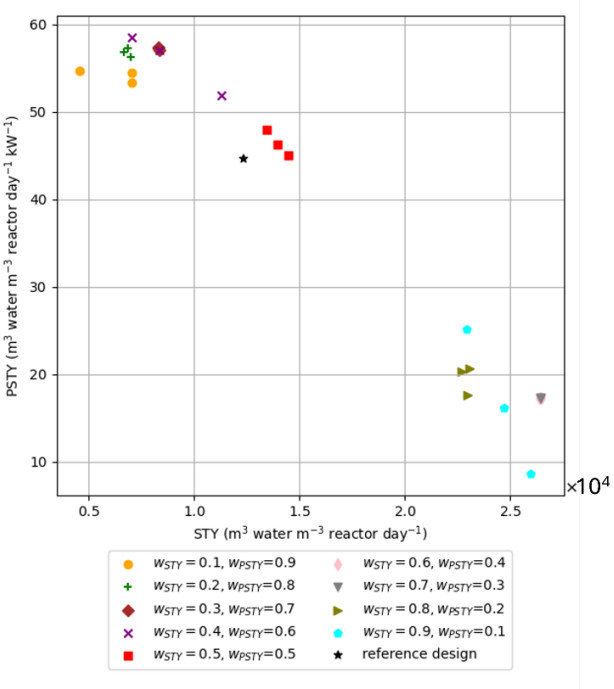

Figure 3. effect of weights on STY and PSTY

Following the investigation on the weight effect, a BO optimization with 50 random points and 150 additional simulations was conducted. All candidate points are shown in Figure 4. The STY ranges from approximately 5,000 to 22,500 m³ water/m³ reactor/day, while the PSTY ranges from about 15 to 60 m³ water/m³ reactor/day/kW. As expected, a negative correlation between STY and PSTY is observed, indicating a trade-off between these two parameter. The results are compared to the reference design, shown with a black marker: three unit cells

with 2 mm diameter circular channels, as described by Jacobs et al. [6]. A general trend is observed where larger PSTY values correspond to increased channel volumes. This is attributed to a greater amount of photocatalyst, which can absorb more light energy. However, designs with similar volumes may vary in the amount of absorbed light, demonstrating the impact of geometrical configuration.

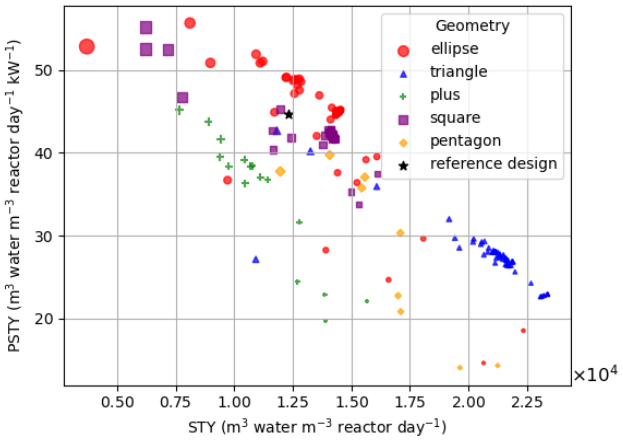

Figure 4. Bayesian optimization results (marker sizes proportional to channel volumes.)

Triangular channels are predominantly located in the bottom-right corner of Figure 4, where the STY is maximized. For pentagonal and plus-shaped channel geometries, the results are relatively suboptimal compared to the other geometries. Square channels are positioned in the middle and upper-left regions of the figure, showing some of the highest PSTY values. Elliptic channels dominate the balanced region and are clustered around the reference design, indicating promising solutions.

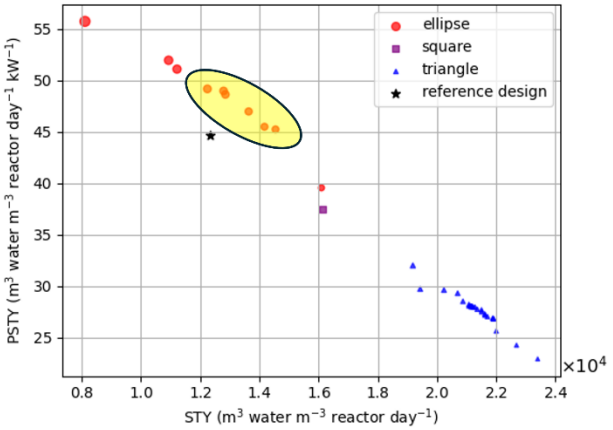

Figure 5. Pareto optimal solutions with dominating solutions indicated by the yellow area.

The Pareto front, which represents the non-dominating designs, is plotted separately in Figure 5. Dominating solutions, highlighted in yellow, include points that outperform the reference design in both objectives, as well as those that are slightly worse in one objective. The exact geometrical configurations of the dominating solutions are detailed in Table 3. Each solution is defined by its characteristic diameter (a), aspect ratio for ellipses only (b/a), rotation angle (r), number of vertically stacked rows (N), and total channel volume (V). All dominating solutions feature an elliptic channel shape, with a consistent aspect ratio (b/a) of 1.75 across all configurations, indicating highly elongated ellipses. The rotation angle (r) ranges from 56.4° to 90.0°, reflecting variations in the orientation of the elliptical geometry within the design. The characteristic diameters fall between 1.00 mm and 1.95 mm despite being examined over a broader range of 1.00 mm to 6.50 mm, suggesting that smaller geometries are more favorable. Table 3 also indicates that an optimal design can be achieved with two vertically stacked rows. At one extreme, the optimization study enables a 15.3% increase in STY with only a 1.2% increase in PSTY. Additionally, a roughly 9.0% increase in PSTY can be achieved with a minor reduction in STY at the other extreme. These findings demonstrate the influence of geometrical configuration on the performance of a photo-reactor, and the results emphasize the importance of considering both reaction efficiency and energy efficiency together in reactor design.

Table 3: Geometrical configurations of the dominating solutions. (**a**: Characteristic diameter/minor axis length for ellipses, **b/a**: Aspect ratio of the ellipse, **r**: Rotation, **N**: Number of vertically stacked rows, **V**: Total volume of channels, **ΔSTY**: Percent change in STY compared to the reference design, **ΔPSTY**: Percent change PSTY compared to the reference design)

a (mm)	b/a	r (°)	N	Shape	ΔSTY (%)	ΔPSTY (%)
1.95	1.75	90.0	2	Ellipse	-0.6	9.1
1.21	1.75	57.1	3	Ellipse	3.6	8.7
1.21	1.75	56.5	3	Ellipse	4.1	8.1
1.10	1.75	56.4	3	Ellipse	9.6	4.8
1.01	1.75	56.5	3	Ellipse	13.0	1.7
1.00	1.75	81.6	3	Ellipse	15.3	1.2

BO is particularly effective for optimizing functions with up to 20 variables. Although this study includes categorical and discrete variables, which make the optimization problem more complex, the total number of variables is much lower than 20. Hence, computational efficiency is not a limiting factor for either BO or the ray tracing simulation, considering that it is a 2D simulation. The proposed methodology can be extended to alternative channel shapes and various types of photoreactors. However, if a more free-form surface controlled by multiple parameters is used, computational

complexity must be considered for 3D simulations, as well as geometrical complexity and reactor dimensions.

CONCLUSION

This study demonstrates the successful application of Bayesian optimization for designing translucent monolithic photochemical reactors. Through a systematic multi-objective optimization approach considering both STY and PSTY, we identified optimal channel geometries that outperform circular designs. The results revealed important trade-offs between STY and PSTY, with elliptical channels showing the best performances. Two optimized elliptical configurations achieved up to 15.3% improvement in STY with minimal PSTY increase and 9.0% enhancement in PSTY with negligible STY decrease. The methodology established here provides a framework for optimizing photochemical reactor designs using ray tracing-coupled Bayesian optimization. The findings demonstrate that geometric optimization can significantly enhance throughput and energy efficiency in translucent monolithic reactors.

ACKNOWLEDGEMENTS

Prof. Leblebici gratefully acknowledges the support of KU Leuven C2 project Scalable performant solar cell module for CO2 Reduction Coupled with Organic Synthesis (SPROUT) C2E/23/010.

REFERENCES

1. Su, Y., Straathof, N. J. W., Hessel, V., & Noël, T. Photochemical transformations accelerated in continuous-flow reactors: Basic concepts and applications. In *Chemistry - A European Journal* (Vol. 20, Issue 34, pp. 10562–10589). Wiley-VCH Verlag. (2014) https://doi.org/10.1002/chem.201400283
2. Loubière, K., Oelgemöller, M., Aillet, T., Dechy-Cabaret, O., & Prat, L. Continuous-flow photochemistry: A need for chemical engineering. *Chemical Engineering and Processing - Process Intensification*, *104*, 120–132. (2016) https://doi.org/10.1016/j.cep.2016.02.008
3. Claes, T., Dilissen, A., Leblebici, M. E., & van Gerven, T. Translucent packed bed structures for high throughput photocatalytic reactors. *Chemical Engineering Journal*, *361*, 725–735. (2019) https://doi.org/10.1016/j.cej.2018.12.107
4. Coyle, E. E., & Oelgemöller, M. Micro-photochemistry: Photochemistry in microstructured reactors. The new photochemistry of the future? In *Photochemical and Photobiological Sciences* (Vol. 7, Issue 11, pp. 1313–1322). Royal Society of Chemistry. (2008) https://doi.org/10.1039/b808778d
5. Leblebici, M. E., Stefanidis, G. D., & van Gerven, T. Comparison of photocatalytic space-time yields of 12 reactor designs for wastewater treatment. *Chemical Engineering and Processing: Process Intensification*, *97*, 106–111. (2015) https://doi.org/10.1016/j.cep.2015.09.009
6. Jacobs, M., Meir, G., Hakki, A., Thomassen, L. C. J., Kuhn, S., & Leblebici, M. E. Scaling up multiphase photochemical reactions using translucent monoliths. *Chemical Engineering and Processing - Process Intensification*, *181*. (2022) https://doi.org/10.1016/j.cep.2022.109138
7. Binjhade, R., Mondal, R., & Mondal, S. Continuous photocatalytic reactor: Critical review on the design and performance. In *Journal of Environmental Chemical Engineering* (Vol. 10, Issue 3). Elsevier Ltd. (2022) https://doi.org/10.1016/j.jece.2022.107746
8. Jacobs, M., Meir, G., Hakki, A., Thomassen, L. C. J., Kuhn, S., & Leblebici, M. E. Scaling up multiphase photochemical reactions using translucent monoliths. *Chemical Engineering and Processing - Process Intensification*, *181*. (2022) https://doi.org/10.1016/j.cep.2022.109138
9. Athanasiou, D. A., Romanos, G. E., & Falaras, P. Design and optimization of a photocatalytic reactor for water purification combining optical fiber and membrane technologies. *Chemical Engineering Journal*, *305*, 92–103. (2016) https://doi.org/10.1016/j.cej.2015.11.080
10. Martín-Sómer, M., Moreira, J., Santos, C., Gomes, A. I., Moreno-SanSegundo, J., Vilar, V. J. P., & Marugán, J. Reflector design for the optimization of photoactivated processes in tubular reactors for water treatment. *Journal of Environmental Chemical Engineering*, *11*(5). (2023) https://doi.org/10.1016/j.jece.2023.110609
11. Singh, M., Salvadó-Estivill, I., & Li Puma, G. Radiation field optimization in photocatalytic df monolith reactors for air treatment. *AIChE Journal*, *53*(3), 678–686. (2007) https://doi.org/10.1002/aic.11093
12. Savage, T., Basha, N., McDonough, J. Machine learning-assisted discovery of flow reactor designs. *Nat Chem Eng* **1**, 522–531 (2024). https://doi.org/10.1038/s44286-024-00099-1